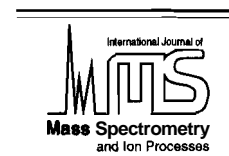




ELSEVIER

International Journal of Mass Spectrometry and Ion Processes 135, (1994) 1–17



Resonance-enhanced multiphoton ionization of argon: reactivity as a probe for the $^2P_{1/2}/^2P_{3/2}$ population¹

M. Schweizer, S. Mark, D. Gerlich*

Fakultät für Physik, Universität Freiburg, 79104 Freiburg, Germany

(Received 27 October 1993; accepted 22 November 1993)

Abstract

The guided ion beam (GIB) technique is not only well suited for determining precise integral cross-sections but is also useful for analyzing state populations in simple systems based on their chemical reactivity. In this paper, the method has been applied to characterize some multiphoton ionization schemes via different resonant intermediates of Ar utilizing the endothermic charge-transfer reaction $\text{Ar}^+ + \text{O}_2 \rightarrow \text{O}_2^+(a) + \text{Ar}$ as a probing reaction. Cross-sections measured in the threshold region indicate that ionization via the $\text{Ar}(4s'[1/2]_1)$ and $\text{Ar}(4p'[3/2]_2)$ states leads to $\text{Ar}^+(^2P_{3/2})$ and $\text{Ar}^+(^2P_{1/2})$ production with a purity of $(97 \pm 3)\%$ and $(95 \pm 5)\%$, respectively, whereas other transitions lead to mixtures. Additional studies of collisions between state-selected Ar^- ions with N_2 , H_2 and D_2 and comparison with published values not only corroborate these conclusions but also provide new state-specific information for these systems, especially at low collision energies.

Key words: Resonance-enhanced multiphoton ionization; State-selected ion/molecule reactions; Charge transfer; Guided ion beam, Ar^+ ions

1. Introduction

Many attempts have been made in the last two decades to measure very detailed cross-sections for collision processes. One of the goals of such studies is, for example, to find specific forms of energy which influence predominantly the outcome of a chemical reaction. A more fundamental aim is to understand the dynamics of the interaction between the reac-

tants from first principles and to develop theoretical methods which are able to predict the experimental results. For critical comparisons between theory and measurement very accurate state-to-state cross-sections are needed. Although the expression state-to-state has been in use many years, there are few experiments where the states of the reactants are prepared as well as those of the products are analyzed.

For preparing ionic reactants suitable properties of the ionization process itself can be utilized. Among the various methods such as electron bombardment, chemi-ionization or photoionization, the last one has the largest potential. Single-photon ionization with

*Corresponding author. New address: Fakultät für Naturwissenschaften, Technische Universität Chemnitz-Zwickau, PF 964, D09009 Chemnitz, Germany.

¹ Dedicated to Professor Christoph Ottinger on the occasion of his 60th birthday.

monochromatic VUV photons from a continuous discharge lamp was pioneered by Chupka and Russell [1]; today in most instances synchrotron radiation or VUV lasers are applied. Alternatively one can combine the energy of several photons for ejecting a single electron. This has the advantage that the required wavelength is in the visible or near UV region, where intense laser sources are available. If one uses, in addition, excitation via a resonant intermediate state, ions can be produced with high efficiency and also in states which otherwise cannot be reached.

Photoionization methods have the advantage that the manifold of formed states can be limited by energy constraints or restricted by propensity or selection rules, in particular if resonant intermediates or autoionizing levels are involved. Nonetheless in most situations, it is advisable to analyze the state distribution of the formed ion ensemble, e.g. by recording a photoelectron spectrum (PES). If ionization with monochromatized photons leads to ions in several states, one can pick out individual ones by coincidence techniques, correlating one ion with one energy-selected photoelectron. Especially well suited for this purpose are threshold electrons and first promising developments have also been reported with zero-kinetic-energy photoelectrons [2]. The high-energy resolution of this technique allows one to prepare molecular ions in selected rotational states [3].

If one uses for ionization other methods than photoionization the state of the created ion cannot be determined by electron spectroscopy. There are also other approaches to influence the state population of reactants such as chemical quenching, thermalization of an ensemble at various temperatures (in particular at low ones), optical excitation and laser pumping. In all these instances more general methods are needed to analyze the resulting populations; e.g. based on lasers or chemical probing techniques. The last technique

has been used for many years to characterize autoionizing transitions in H_2 [1] and it is applied routinely in drift tube experiments for analyzing reaction products [4, 5]. More recently this approach has also been combined successfully [6] with the guided ion beam (GIB) technique which is known to be a powerful method for determining precise integral cross-sections [7], in particular, in combination with VUV and multiphoton ionization sources [8, 9].

In this paper we discuss the potential but also the limitations and problems of the GIB technique for determining state-specific cross-sections and for probing ionic states by chemical reactions. As a test case we use a simple two-state mixture of Ar^+ ions prepared by resonance-enhanced multiphoton ionization (REMPI) via several intermediates. Reactions of these ions with several molecules are examined for the specific purpose of seeing whether they are suited for determining the $^2\text{P}_{1/2} : ^2\text{P}_{3/2}$ fine-structure ratio of the Ar^+ reactants.

It should be noted that in the present experiment the ion ensemble is probed by collisions in the same scattering cell which is otherwise used to determine state-specific cross-sections. This has the advantage that collisional relaxation is accounted for, as is radiative decay or fragmentation of molecular ions en route to the interaction region. In the specific case of REMPI the in situ analysis is also superior to electron spectroscopy in certain respects. Here the electron energy distribution may be perturbed and the ion state population can depend critically on parameters such as laser power density. It is therefore problematic to transfer results from one experiment to another.

2. Experimental

2.1 Instrumental details

The experiment was performed in a well

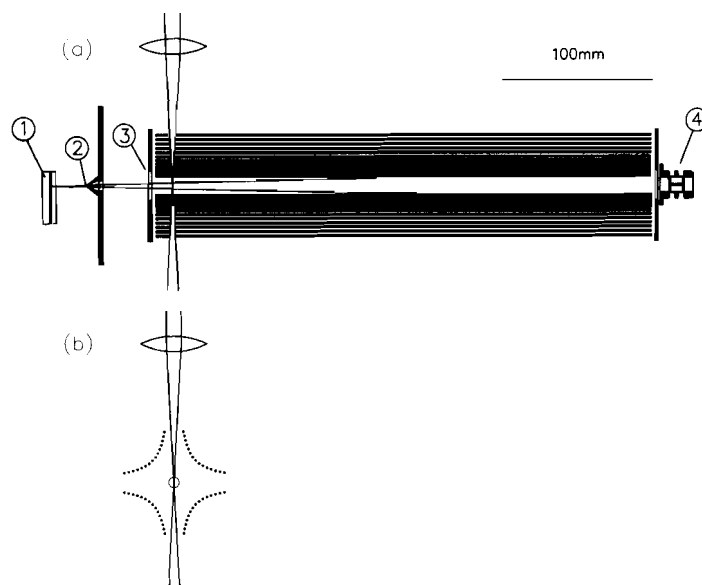


Fig. 1. **Quadrupole** photoionization source. Part (a) shows the most important features in the plane which is formed by the laser beam, the gas beam and the quadrupole axis: (1) piezoelectric valve, (2) skimmer, (3) ion repeller, (4) exit ion lens. Part (b) illustrates that the hyperbolic boundary conditions of the **quadrupole** field are approximated by four groups of 15 rods each. For diagnostic purposes, ionization is also possible with an electron beam which is perpendicular to the laser beam.

characterized GIB apparatus which has been described in detail elsewhere [7]. One of the outstanding features of this machine is that it can be used to measure absolute values for integral cross-sections with high accuracy from thermal energies to several electronvolts.

The main modification for the present study concerns the ion production. Figure 1 shows a sketch of the photoionization source. The ions are created inside a linear r.f. quadrupole. The hyperbolic boundary conditions of this device are approximated by 4 x 15 rods with diameter 1 mm which are arranged as depicted in Fig. 1. The inscribed circle of this structure has a diameter of 40 mm. This rather large dimension has been chosen to reduce the influence of surface potential distortions in the vicinity of the center line of the quadrupole where the ions move. Another advantage of the open construction is that the neutral precursor gas can be pumped away efficiently.

The use of an r.f. guiding field in a photoionization source has the advantage of high

collection and transmission efficiency. In addition, the mass- and energy-dependent focusing properties of the harmonic effective potential [7] allow us to prepare a primary beam with a very narrow translational energy distribution. We succeeded in producing an ion beam with an axial energy of only 30 meV and with an energy half width of 2 meV. In the present study the quadrupole has been operated in a less selective mode using higher guiding field strength. The resulting energy half width, $\Delta E_T = 25 \text{ meV}$, is still smaller than the overall energy resolution which is determined by other effects such as the thermal target gas motion. For preparation of an Ar^+ ion beam we have used a frequency of $\Omega = 2\pi \times 2.4 \text{ MHz}$, an amplitude of $V_0 = 245 \text{ V}$ and an axial kinetic energy of 1 eV.

The ionizing laser (30 Hz Quantel Nd:YAG pumped dye laser with doubling and mixing) passes through the quadrupole perpendicularly and intersects the molecular beam on the axis of the ion guide (see Fig. 1). The

Table 1

REMPI of Ar using several intermediate states. Columns give the required wavelength, the number of photons, the cross-section measured for the $\text{Ar}^+ + \text{O}_2$ charge-transfer system at 0.4 eV and the fraction of $^2\text{P}_{3/2}$ ground-state ions determined for the indicated transitions

Configuration	Designation	$\lambda(\text{nm})$	REMPI	$\sigma(\text{O}_2^+, 0.4\text{eV})(\text{\AA}^2)$	Fraction $^2\text{P}_{3/2}$
$3\text{p}^5(^2\text{P}_{1/2}^0)4\text{s}$	$4\text{s}' [1/2]_1$	314.5	3 + 1	0.4 ± 0.1	0.97 ± 0.03
$3\text{p}^5(^2\text{P}_{3/2}^0)4\text{s}$	$4\text{s} [3/2]_1$	320.0	3 + 2	1.2 ± 0.1	0.51 ± 0.08
$3\text{p}^5(^2\text{P}_{3/2}^0)4\text{p}$	$4\text{p} [5/2]_2$	378.7	4 + 1	–	–
$3\text{p}^5(^2\text{P}_{3/2}^0)4\text{p}$	$4\text{p} [3/2]_2$	376.5	4 + 1	–	–
$3\text{p}^5(^2\text{P}_{3/2}^0)4\text{p}$	$4\text{p} [1/2]_0$	373.6	4 + 1	1.0 ± 0.1	0.64 ± 0.08
$3\text{p}^5(^2\text{P}_{1/2}^0)4\text{p}$	$4\text{p}' [3/2]_2$	372.8	4 + 1	2.1 ± 0.2	0.05 ± 0.05
$3\text{p}^5(^2\text{P}_{1/2}^0)4\text{p}$	$4\text{p}' [1/2]_0$	367.9	4 + 1	–	–
	$\text{e}^- \text{ impact}$			1.0 ± 0.1	2/3

light beam is focused by a 10 cm lens. For 3 + 1 and 3 + 2 REMPI of Ar the dye laser has been operated with DCM. By doubling the output a wavelength between 314 and 320 nm has been obtained with an energy of 2 mJ per pulse and a resolution of 0.08 cm^{-1} . For 4 + 1 REMPI a mixture of Rh B and Rh 6G has been used. Mixing the output of the dye laser with the fundamental of the YAG leads to 373 nm with an energy of 8 mJ per pulse. Since there was no interactivity etalon in the YAG laser the resolution of the mixed laser beam was only about 1 cm^{-1} . Depending on the imaging and focusing conditions the power density of the laser light in the ionization volume could be varied between 10^7 and 10^9 W cm^{-2} .

The neutral precursor gas is injected coaxially with the quadrupole axis. In order to produce 20–30 ions per laser shot an argon density of about 10^{12} cm^{-3} is required in the laser focus. To achieve this, there are two alternative beam sources, a pulsed supersonic beam as depicted in Fig. 1. or a 1 mm diameter tube ending very close ($\approx 3 \text{ mm}$) to the laser focus. The former has the advantage of cooling the neutral gas during the adiabatic expansion, leading for example to low rotational temperatures. The effusive gas inlet is superior if adiabatic cooling is not necessary, as for atoms, or not desired, e.g. if one needs neutral precursors in high rotational states.

2.2 REMPI of Ar

The ionization potential of Ar lies at 15.760 eV [10]. By spin-orbit interaction the Ar^+ ground state is split into two levels which are separated by $\text{AE} = 177.5 \text{ meV}$. In order to ionize Ar with four or five photons the wavelength must be shorter than 314.69 nm or 393.36 nm, respectively. For a resonant transition via an intermediate with the main quantum number 4 one can select out of a total of seven accessible states (Table 1) resulting in 3 + 1, 3 + 2 or 4 + 1 REMPI schemes [10]. In the present work we have examined only those four transitions which are shown schematically in Fig. 2. With three photons of 320.0 nm or 314.5 nm the $4\text{s} [3/2]_1$ or $4\text{s}' [1/2]_1$ states are reached, while with four photons of 373.6 nm or 372.8 nm we reach the $4\text{p} [1/2]_0$ or $4\text{p}' [3/2]_2$ states, respectively. Note that the illustration uses different scales in different regions, but the relative position of the intermediate states can be compared and the range in the vicinity of the ionization limit (grey area) is at the same scale, too. A typical spectrum for 4 + 1 REMPI measured at a laser power of $5 \times 10^8 \text{ W cm}^{-2}$ is shown in Fig. 3. The asymmetric line shape is due to a.c. stark broadening and varies strongly with the laser power. For example, the half width of the 3 + 1 transition at 314.5 nm has been observed to

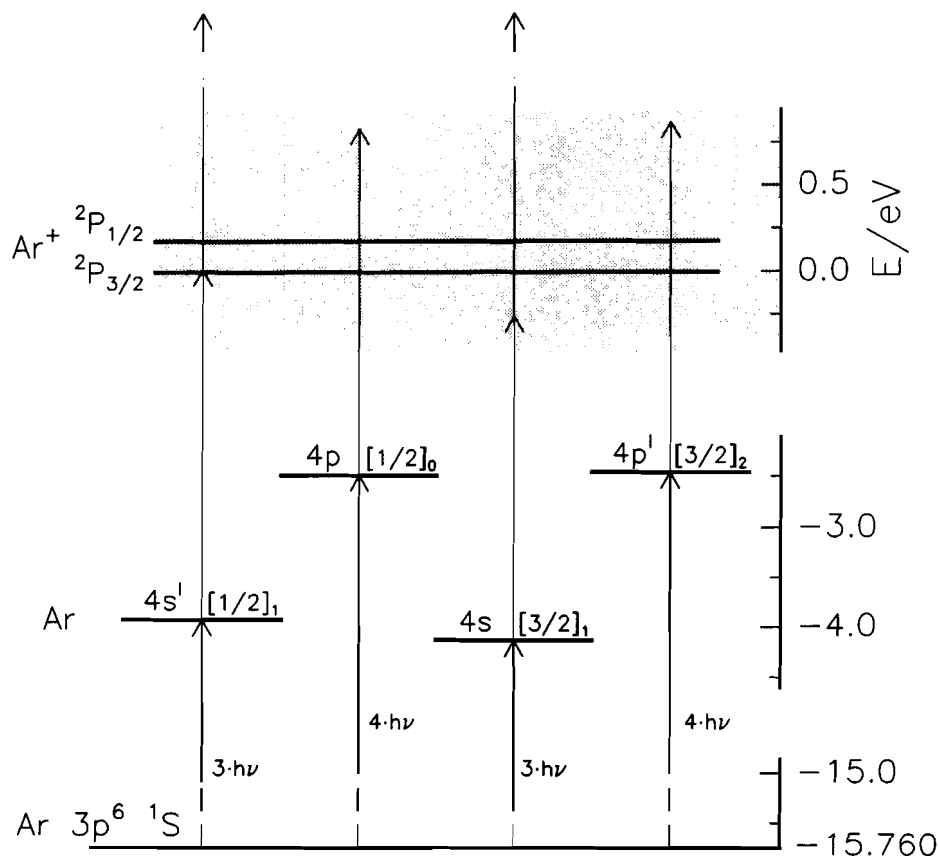


Fig. 2. Resonance-enhanced multiphoton ionization of argon via some intermediate states with the main quantum number 4. Note that the energy scale in the region of the intermediate states is different from that in the vicinity of the ionization limit.

increase from 0.7 cm^{-1} at $2.6 \times 10^7 \text{ W cm}^{-2}$ to 5 cm^{-1} at $2.5 \times 10^9 \text{ cm}^{-2}$.

The most important question for our application is whether there are any obvious criteria for finding a correlation between the intermediate state and the state of the formed ion. In general, propensity rules are based on the assumption that the core of the intermediate state has already $^2\text{P}_{3/2}$ or $^2\text{P}_{1/2}$ character and that this configuration is conserved during the absorption of the subsequent photon. This often holds for Rydberg states but for the main quantum number 4 as in the present example one must expect significant deviations due to electron-electron correlation. Other criteria are based on accidental near-resonances with autoionizing states as in the

case of the $4s'$ transition. For this transition the energy of four photons lies just 11 meV above the ionization limit of the $^2\text{P}_{3/2}$ state, i.e. in the region of Rydberg states which converge to the $^2\text{P}_{1/2}$ state (see Fig. 2). Transitions via this path can compete with the absorption of a fifth photon, which means that fine-structure changing (near-) autoionization can compete with $^2\text{P}_{1/2}$ core-preserving ionization.

Photoelectrons from these two processes have very different energies, 11 meV and 3.78 eV, and, disregarding discrimination effects, the detection of the two groups of electrons should be no problem with a simple photoelectron spectrometer. Unfortunately, almost no PES work on Ar multiphoton ionization has been reported, and there is

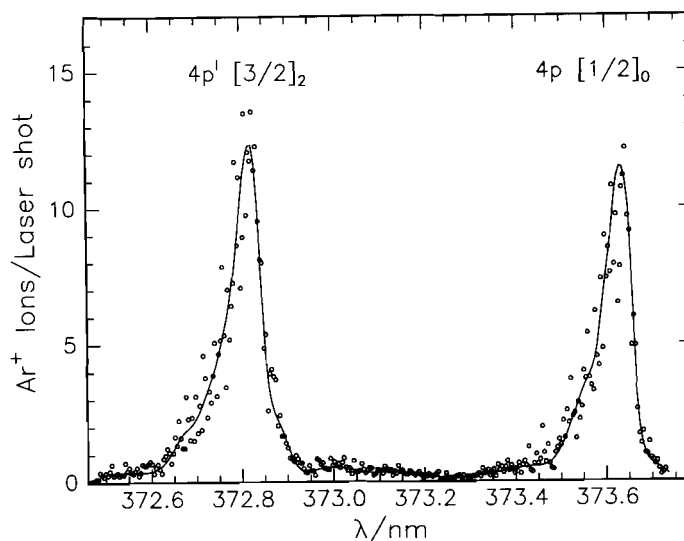


Fig. 3. 4 + 1 REMPI spectrum of argon via $4p'$ and $4p$ recorded with a laser power density of $5 \times 10^8 \text{ W cm}^{-2}$ in the focus. A curve has been superimposed for help with visualization.

especially no information on excitation via the $4p$ or the $4p'$ intermediate. Some notes on electron spectra from transitions via the $4s'$ and the $4s$ intermediate can be found in the Ph.D. thesis of Bajic [11]. Orlando et al. [12] have ionized Ar, mainly for calibration purposes, via the $4s'$ intermediate. For this transition both studies conclude from the electron energy distribution that there is a strong preference for forming Ar^+ in the $^2\text{P}_{3/2}$ ground state, which is energetically possible with a $3 + 1$ process. We have corroborated the fact that in this instance only four photons with 314.5 nm are utilized for ejecting the electron by examining the dependence on the laser power P . For this transition ionization is very efficient and varies proportionally with $P^{1.6}$, whereas all other transitions produce fewer ions and the yield depends much more strongly on the laser intensity since at least five photons are necessary.

Due to the lack of PES data and for further characterization of the various REMPI processes we have used our GIB apparatus, and studied the reactivity of the produced Ar^+ ions in collisions with molecules such as O_2 , N_2 , H_2

and D_2 . In these studies, the charge-transfer system of $\text{Ar}^+ + \text{O}_2$ plays a central role since it is, among others, one of the best and most recently examined systems [8, 13, 14].

3. Results and discussion

3.1 Calibration of the fine-structure state population

It is known from measurements in a flow-drift tube [15] that the rate coefficient of the charge-transfer system $\text{Ar}^+ + \text{O}_2$ has a pronounced energy dependence. At room temperature it has only about 10% of the Langevin limit. With increasing energy the rate coefficient drops steeply and reaches a minimum at a collision energy of about 0.3 eV. Up to this energy, only the exothermic reaction channel $\text{Ar}^+ + \text{O}_2 \rightarrow \text{O}_2^+(\text{X}) + \text{Ar}$ can contribute to O_2^+ formation. The significant increase at collision energies above 0.3 eV is caused by the opening of the endothermic channel $\text{O}_2^+(\text{a}) + \text{Ar}$. Experiments with state-selected ions [13, 16] have shown that in this

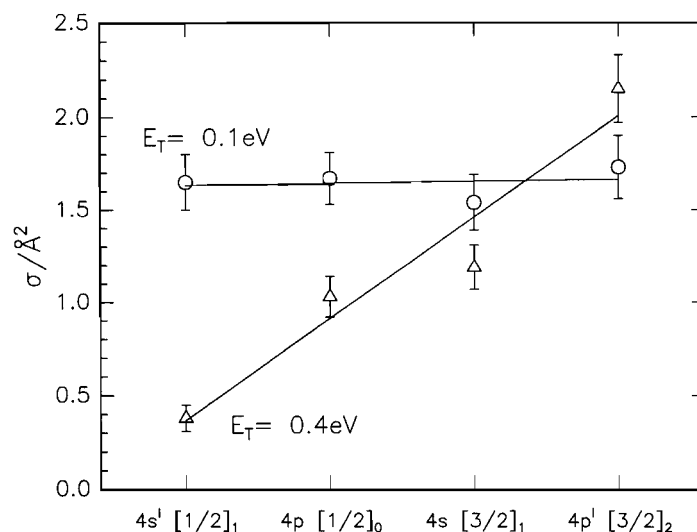


Fig. 4. Integral cross-sections for the charge-transfer reaction $\text{Ar}^+ + \text{O}_2 \rightarrow \text{O}_2^+ + \text{Ar}$ measured at $E_T = 0.1$ and 0.4 eV for the four ionization pathways depicted in Fig. 2. The observations are in accordance with the fact [13, 16] that at low energies the integral cross-section is independent of the Ar^+ fine-structure state whereas at energies in the threshold region for forming $\text{O}_2^+(\text{a})$ ions, excited Ar^+ ions are more reactive.

energy range the integral cross-section depends on the fine-structure state of Ar^+ whereas it is independent of this at low energies.

These observations have also been reproduced for Ar^+ ions created by REMPI, first in a more qualitative way. Figure 4 shows a few typical results for two collision energies, $E_T = 0.1 \text{ eV}$ and $E_T = 0.4 \text{ eV}$. The cross-sections are plotted for the four different ionization paths depicted in Fig. 2. At $E_T = 0.1 \text{ eV}$ they all have the same value within the error bars, whereas, at $E_T = 0.4 \text{ eV}$ a significant dependence on the transition is obvious. This behavior has been used to calibrate the population of the fine-structure states $^2\text{P}_{3/2}$ and $^2\text{P}_{1/2}$ in the prepared Ar^+ ion beam. The individual steps of the calibration procedure are described below.

First the measured cross-section has been corrected for contributions from $\text{O}_2^+(\text{X})$ production. For this purpose $\sigma(E_T)$ has been recorded from thermal energies to a few electronvolts. The results are depicted in Fig. 5. In order to separate the $\text{O}_2^+(\text{X})$ and $\text{O}_2^+(\text{a})$ channel and to account for the thermal broadening,

the data points have been fit by the weighted sum of two empirical analytical functions (broken lines) representing the cross-section for individual channels. The solid lines represent effective cross-sections calculated with weighted sums of these three functions and taking into account the thermal 300 K target gas motion [17].

Figure 5(a) presents results for $3 \rightarrow 1$ REMPI via $4s' [1/2]_1$ and $4 \rightarrow 1$ REMPI via $4p' [3/2]_2$. These are the two transitions where the reactivity of the resulting Ar^+ ions is the least and the most, respectively. The low-energy part of the cross-section, where only ground-state $\text{O}_2^+(\text{X})$ ions are energetically accessible, has been described with the ansatz already reported by Scherbarth and Gerlich [14], however with slightly different parameters (broken line in Fig. 5):

$$\sigma = 0.09(E_T/\text{eV})^{-1.22} \quad (1)$$

In accordance with other experiments [13, 16] our results also show that this exothermic charge-transfer channel does not depend on fine-structure energy, which can be taken as

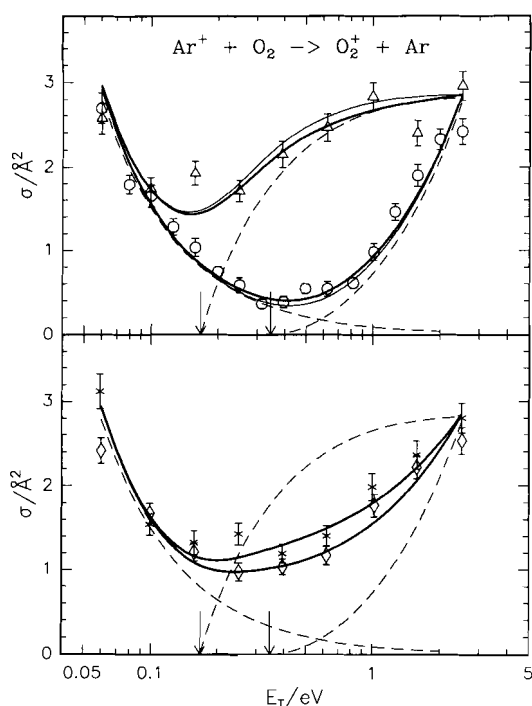


Fig. 5. Integral cross-sections for the charge-transfer reaction $\text{Ar}^+ + \text{O}_2 \rightarrow \text{O}_2^+ + \text{Ar}$ as a function of collision energy for four different ways to prepare Ar^+ ions by REMPI. Upper panel: $3 + 1$ REMPI via $4s' [1/2]_1$ (O) and $4 + 1$ REMPI via $4p' [3/2]_2$ (Δ); Lower panel: $3 + 2$ REMPI via $4s [3/2]_1$ (x) and $4 + 1$ REMPI via $4p [1/2]_0$ (O). The solid lines are effective cross-sections calculated using weighted sums of the analytical cross-sections shown as broken lines. The weights for the bold lines are given in Table 1, the thin solid lines are predictions for pure Ar^+ states.

an experimental hint that fine-structure energy and translational energy are not equivalent. By subtracting the part described by Eq. (1) from the measured values, the specific cross-sections for forming $\text{O}_2^+(\text{a})$ are obtained. These results show thresholds, which are consistent with the theoretical values for the two Ar^+ fine-structure states, indicated in Fig. 5 by the arrows. In detail we calculate, at 0.4 eV , in one instance a low value of $0.1 \pm 0.1 \text{ \AA}^2$ which shows that photoionization via $4s' [1/2]_1$ is predestinated for $^2\text{P}_{3/2}$ production. For photoionization via $4p' [3/2]_2$ the created ion ensemble leads to $1.9 \pm 0.2 \text{ \AA}^2$, indicating that this transition

predominantly produces the $^2\text{P}_{1/2}$ state of the Ar^+ . Since only two ionic states are accessible both measured cross-sections are linear combinations of $\sigma_{3/2}$ and $\sigma_{1/2}$. Therefore a first estimate of the maximum $^2\text{P}_{1/2}$ impurity can be simply achieved for that ion ensemble which reacts with 0.1 \AA^2 . With the assumption that this cross-section is exclusively due to Ar^+ ions in the excited $^2\text{P}_{1/2}$ state and with the knowledge that the $^2\text{P}_{1/2}$ ions react with a cross-section larger than the measured 1.9 \AA^2 one obtains for this impurity a value below 6%.

In order to estimate the fractional abundance of $\text{Ar}^+(^2\text{P}_{3/2})$ for the $4p' [3/2]_2$ intermediate the cross-section is compared with that for a statistical mixture of both spin-orbit states. Since a comparison of absolute values determined using different machines under different conditions is not trivial we have remeasured a reliable absolute cross-section by using electron bombardment, but otherwise identical experimental conditions. For that purpose the ions have been created using an electron beam instead of the laser beam. At an electron energy of 60 eV it is safe to assume that the two fine-structure states are populated in their statistical weight, $^2\text{P}_{3/2} : ^2\text{P}_{1/2} = 2 : 1$. With this mixture we have measured a cross-section of $1.0 \pm 0.1 \text{ \AA}^2$ at $E_T = 0.4 \text{ eV}$ which is, within the error bars, consistent with the value published by Scherbarth and Gerlich [14]. Assuming again the extreme case that $^2\text{P}_{3/2}$ ground-state ions do not react we find, as a first characterization of the $4p'$ transition, that more than 86% of the produced ion ensemble is in the $^2\text{P}_{1/2}$ state.

For a more quantitative analysis, the threshold regions of the endothermic cross-section to form $\text{O}_2^+(\text{a})$ have been approximated with an ansatz, using the line of center model:

$$\sigma = \sigma_0(E_T - E_0)/eV^n / E_T/eV \quad (2)$$

As can be seen from Fig. 5 a set of parameters has been found which lead to good overall

agreement with the experimental data. For the $^2P_{3/2}$ ground state (threshold $E_0 = 0.345 \text{ eV}$) we have obtained a slow onset with $n = 1.90$ and $\sigma_0 = 1.60 \text{ \AA}^2$, whereas for $^2P_{1/2}\text{Ar}^+$ ions ($E_0 = 0.167 \text{ eV}$), the cross-section increases more steeply with $n = 0.95$ and $\sigma_0 = 3.15 \text{ \AA}^2$. These different threshold behaviors (see Fig. 5) which indicate different efficiencies for using the fine-structure energy, can be understood qualitatively with the simple reaction model discussed by Scherbarth and Gerlich [14]. Within that model, translational energy has to be transferred into vibrational excitation of the O_2 molecule by an intimate collision, before the charge transfer to the $\text{O}_2^+(\text{a})$ become energetically accessible during the dissociation of the collision complex. Starting with $^2P_{1/2}$ on the upper fine-structure surface, less translational energy must be converted, which may explain the steeper cross-section onset for formation of $\text{O}_2^+(\text{a})$. This argument is based on the assumption that non-adiabatic coupling is similar for both manifolds of surfaces converging asymptotically to the two fine-structure states.

To illustrate the sensitivity and the limits of our method in determining the fine-structure population, Fig. 5(a) shows the two effective cross-sections for a beam of pure, i.e. 100% state-selected ions (thin solid lines) and for ion beams with impurities of a few percent (bold solid lines). The best overall agreement with the data points has been obtained by assuming a $^2P_{3/2}:^2P_{1/2}$ ratio of 97:3 for the 4s' transition and of 5:95 for the 4p' transition. Summarizing it can be concluded that these two transitions lead to almost pure preparation of Ar^+ in the $^2P_{3/2}$ and $^2P_{1/2}$ fine-structure state: the determined deviations have the same magnitude as the errors (see Table 1).

On the basis of the preceding discussions we propose to use the following functions for the state-to-state cross-sections of the $\text{Ar}^+ + \text{O}_2$

charge transfer as a calibration standard:

$$\begin{aligned}\sigma[^2P_{3/2} \rightarrow \text{O}_2^+(\text{X})] &= \sigma[^2P_{1/2} \rightarrow \text{O}_2^+(\text{X})] \\ &= 0.09 \text{ \AA}^2 \times (E_{\text{T}}/\text{eV})^{-1.22}\end{aligned}\quad (3)$$

$$\begin{aligned}\sigma[^2P_{3/2} \rightarrow \text{O}_2(\text{a})] &= 1.60 \text{ \AA}^2 \\ &\times (E_{\text{T}}/\text{eV} - 0.345)^{1.90}/E_{\text{T}}/\text{eV}\end{aligned}\quad (4)$$

$$\begin{aligned}\sigma[^2P_{1/2} \rightarrow \text{O}_2(\text{a})] &= 3.15 \text{ \AA}^2 \\ &\times (E_{\text{T}}/\text{eV} - 0.167)^{0.95}/E_{\text{T}}/\text{eV}\end{aligned}\quad (5)$$

Accounting for the individual experimental influences, these functions allow one to determine the fine-structure state distribution in any other experiment where the primary ions are created in an unknown mixture of the two states. As an example we use the cross-sections shown in Fig. 5(b). They have been measured with Ar^+ ions produced by $3+2$ REMPI via 4s and by $4+1$ REMPI via 4p. The data are in good agreement with the heavy lines calculated from the analytical functions (3)–(5) (broken lines) using the following weighting factors. For ionization via 4s, 51% of the resulting ions are assumed to be in the $^2P_{3/2}$ state, for ionization via $4p[1/2]_0$ the comparison leads to a slightly higher percentage of 64%. The uncertainties of these two results are about $\pm 8\%$. In both instances the population distributions are close to the statistical 2:1 mixture created with electron bombardment.

For a simple quick test we propose to measure the effective cross-section at 0.4 eV (300 K target temperature) and subtract from this value that for X-state formation using the effective value

$$\begin{aligned}\sigma_{\text{eff}}[^2P_{3/2} \rightarrow \text{O}_2^+(\text{X})] &= \sigma_{\text{eff}}[^2P_{1/2} \rightarrow \text{O}_2^+(\text{X})] \\ &= 0.277 \text{ \AA}^2\end{aligned}\quad (6)$$

From the remaining value one can determine the population distribution of the Ar^- ion beam, using the two state-to-state cross-sections at $E_T = 0.4 \text{ eV}$.

$$\sigma_{\text{eff}}[{}^2\text{P}_{3/2} \rightarrow \text{O}_2^+(\text{a})] = 0.065 \text{ \AA}^2 \quad (7)$$

$$\sigma_{\text{eff}}[{}^2\text{P}_{1/2} \rightarrow \text{O}_2^+(\text{a})] = 2.021 \text{ \AA}^2 \quad (8)$$

The effective cross-sections measured in this work for the four REMPI schemes at $E_T = 0.4 \text{ eV}$ are given in Table 1. Note that the ${}^2\text{P}_{3/2}$ fraction given in the last column of this table has been derived from the overall agreement with all measured data and not from the local values given in Eqs. (6)–(8). Applying this test to the cross-section, $\sigma_{\text{eff}} = 1.2 \pm 0.2 \text{ \AA}^2$, reported in Ref. 14, it can be concluded that these experiments have been performed with an ion ensemble very close to the statistical mixture.

3.2 Comparison with other results

As already discussed above, only the PES studies from Orlando et al. [12] and Bajic [11] give any hints concerning the ionic states formed by multiphoton ionization of Ar. For ionization via the $4s'$ intermediate these and our experiments lead consistently to the conclusion that the large majority of Ar^+ ions are formed in the fine-structure ground state. There is, however a significant disagreement for ionization via the $4s$ state. While our measurements clearly indicate a mixture of both spin-orbit states which is very close to the statistical weight, Bajic mentions only one group of photoelectrons corresponding to the ground state [11]. This may be due to the limited energy resolution ($\approx 0.15 \text{ eV}$) of the electrostatic energy analyzer [18] which probably failed to separate the two peaks lying at nominal energies of 3.61 and 3.44 eV. A reinvestigation of the REMPI photoelectron energy spectra at 320 nm may solve this discrepancy. It would also be interesting to provide

the missing information for the other transitions in the 370 nm region.

Another possibility to cross check our results is to use published state-specific cross-sections for other $\text{Ar}^+({}^2\text{P}_j) + \text{X}$ collision processes, some of which have been discussed in a recent review by Ng [8]. However, a huge problem in that comparison is that our method of determining the state population relies on the precision of absolute cross-sections and different experimental methods often lead to different values. In order to limit these problems we have restricted our comparison predominantly to results which have been obtained with GIB machines since with this technique one can achieve a real 4π collection efficiency. But even then we were faced with rather large discrepancies and therefore we decided to further restrict the following figures only to relative values of $\sigma_{1/2}/\sigma_{3/2}$. In this way some of the errors can be eliminated.

It should be emphasized that it is not the aim of the following section to discuss the reaction dynamics of the examined systems in detail. A few related hints only are given where the dynamics are important for understanding the influence of the fine-structure energy.

3.3 $\text{Ar}^+ + \text{O}_2$

State-selected cross-sections for the charge-transfer system $\text{Ar}^+ + \text{O}_2$ have been studied already over a wide energy range by Ng and co-workers [16] and by Dutuit et al. [13]. For comparison their measured values $\sigma_{1/2}/\sigma_{3/2}$ are plotted in Fig. 6 as open symbols. The error bars of our data, shown as solid symbols, include the uncertainty of the state purity discussed above. The broken line represents the ratio that has been calculated directly from a weighted linear combination of the analytical functions (3)–(5). The weights account for our slightly imperfect state preparation, i.e. are based on the experimentally

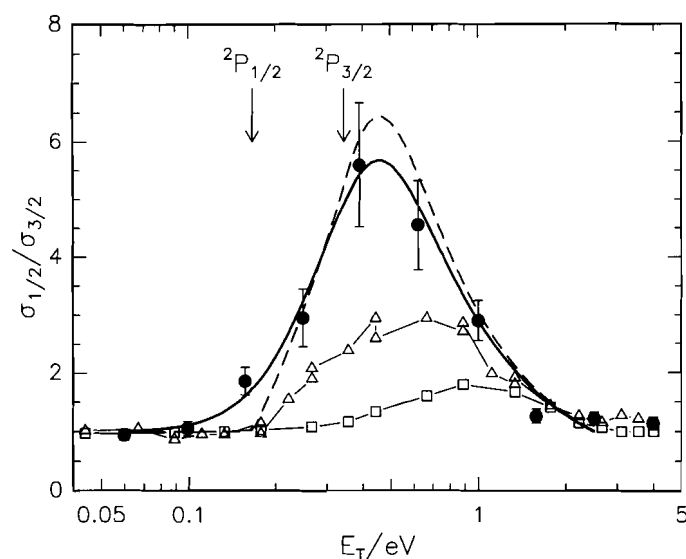


Fig. 6. Ratio of the cross-sections $\sigma_{1/2}$ and $\sigma_{3/2}$ for the charge-transfer system $\text{Ar}^+(\text{}^2\text{P}_j) + \text{O}_2$ as a function of the collision energy, measured by several groups: Ng and co-workers [16] (\square); Dutuit [37] (\triangle); this work (\bullet). The broken and the solid lines have been calculated from the corresponding curves shown in Fig. 5. The arrows mark those collision energies which are required to form $\text{O}_2^+(\text{a})$ in charge transfer with the given Ar^+ state.

determined $\text{}^2\text{P}_{3/2}$ and $\text{}^2\text{P}_{1/2}$ admixtures given in Table 1. If one includes in the calculation also the thermal broadening caused by the target motion, the threshold onset is smeared out and the peak is flattened as can be seen from the solid line. Note that the experimentally determined ratios depend strongly on minor $\text{}^2\text{P}_{1/2}$ admixtures in the ground-state beam and also on the contribution of the cross-section for forming $\text{O}_2^+(\text{X})$, given by Eq. (3). For well prepared beams and without target motion Eqs. (3)–(5) predict a maximum slightly above 8.

It is obvious that there are significant differences between the results of the three groups, concerning both the maximum and its position. In our measurements its value rises to a maximum of 5.5 ± 1 at $E_T = 0.4 \text{ eV}$ while Dutuit et al. [13] found a value of 3 and Flesch et al. [16] only 1.8 at higher collision energies. The discrepancies between the three experiments are even more serious if one compares the absolute values of the cross-sections. For example at $E_T = 0.4 \text{ eV}$ and for ground-state

Ar^+ ions, Flesch et al. have reported a cross-section as large as 3.9 \AA^2 , Dutuit et al. have measured 1.3 \AA^2 while our value is only 0.4 \AA^2 . What are the reasons for these huge discrepancies? In all our experiments there is almost no doubt about the purity of the prepared states. It is also impossible that the ion beam energy widths are responsible for smearing out the structure. The most probable reason we consider is based on the influence of electrostatic potential barriers, which are created by surface potential distortions and which have been found to reach heights up to 100 mV along the axis of the octopole [7].

The following explanation is based on the experimental observation that a small fraction of the primary Ar^+ ions can be trapped in the scattering between such barriers if they lose enough energy by inelastic collisions. It is not easy to get a quantitative estimate of this effect since the fraction of trapped ions not only depends on the potential distortions but also on the conditions in which the ions are injected into the octopole. The energy

distribution of the Ar^+ beam also plays a significant role; in particular, one has to ensure that the distribution does not have a tail extending to very low energies. Since in most experiments the density in the scattering cell is between 10^{12} and $10^{13} \text{ O}_2 \text{ cm}^{-3}$ and due to the Ar/O_2 mass ratio which favors an efficient energy exchange in an inelastic collision, one can easily scatter and trap a few parts per thousand of Ar^+ ions. These thermalized Ar^+ ions can very efficiently charge transfer to O_2^+ , since at these energies the rate coefficient is close to $10^{-10} \text{ cm}^3 \text{ s}^{-1}$ for both fine-structure states and trapping times longer than milliseconds are easily achieved. Under these conditions, trapping of only 2‰ of the Ar^+ ions is sufficient to explain the measured cross-section of Dutuit et al. [13] whereas in Ng's apparatus, less than 6‰ are required to reach an apparent cross-section of 3.9 \AA^2 .

The proposed trapping mechanism can not only explain the discrepancies in the size of the cross-section but also the differences in the $\sigma_{1/2}/\sigma_{3/2}$ ratio depicted in Fig. 6. Since the reactivity of the thermalized Ar^+ ions is independent of their fine-structure state, Flesch et al. who appear to have the largest contribution from trapped ions, found the smallest $\sigma_{1/2}/\sigma_{3/2}$ ratio, while the results obtained by Dutuit et al. are in between ours and those of Flesch.

To further corroborate these speculations we have performed experimental tests to demonstrate the influence of trapped ions by raising artificial barriers with ring electrodes at the entrance and at the exit of the scattering cell. The location and the electrostatic influence of such electrodes have been described in detail in Ref. 7. We have found that it is possible to change the cross-section by one order of magnitude with potential barriers of 50 meV. However we have also checked our octopole concerning unwanted potential distortions, using the "ion reflection" method described in Ref. 7. These tests have proved

that the potential along the axis of our octopole is flat within 10 meV. Under these conditions trapping of Ar^+ ions by inelastic collisions with target gas at 300K is very unlikely and our measured cross-sections are therefore not significantly affected by these problems.

There do not yet exist theoretical explanations for the measured fine-structure dependence of the system $\text{Ar}^+ + \text{O}_2$. Even the various potential surfaces which are involved are not known or at least not known with sufficient accuracy. Therefore most experimental results were explained simply by models based on asymptotic energy levels [19] and Franck–Condon factors [15, 19, 20] or on unpublished Diatomics In Molecule (DIM) potential surfaces [14]. A more detailed discussion of the $(\text{Ar} + \text{O}_2)^+$ collision system, including the reverse reaction $\text{O}_2^+ + \text{Ar}$, will be given in Ref. 13.

3.4 $\text{Ar}^+ + \text{N}_2$

A second system where fine-structure dependence has been studied is the charge transfer between Ar^+ and N_2 . The overall shape of the energy dependence of the cross-section for this process is comparable to that for $\text{Ar}^+ + \text{O}_2$ except that the position of the minimum is shifted towards lower energies, namely to 18 meV [4]. However, the origin of this structure is quite different. From the fact that at sub-thermal energies the rate coefficient reaches only 10% of the Langevin limit, one can conclude that the charge transfer is hindered by an unknown mechanism, although it is exothermic. With increasing temperature the reaction probability becomes even smaller, which may be explained by the energy dependence of the lifetime from the collision complex. The increase in the rate coefficient at collision energies above 18 meV is due to the opening of a new reaction channel. In contrast to the $\text{Ar}^+ + \text{O}_2$ system where

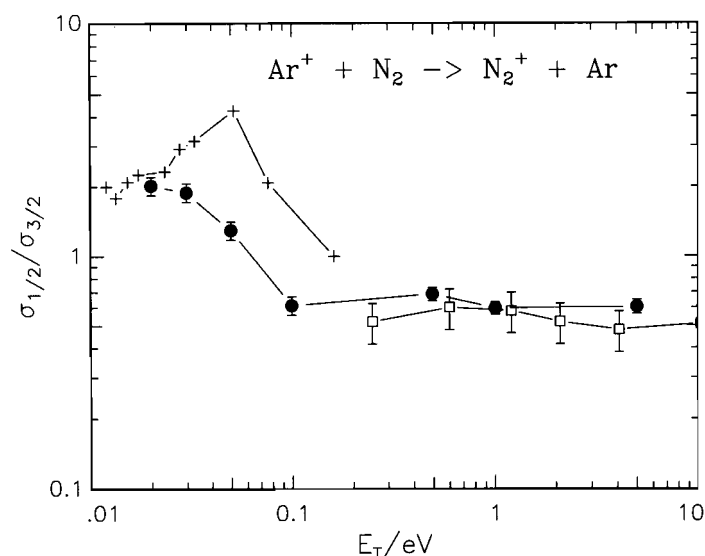


Fig. 7. Ratio of the cross-sections $\sigma_{1/2}$ and $\sigma_{3/2}$ for the charge-transfer reaction $\text{Ar}^+ + \text{N}_2 \rightarrow \text{N}_2^+ + \text{Ar}$ as a function of the collision energy measured by several groups: Ng and co-workers [21] (□); Tobita et al. [22] (+); this work (●). At low collision energies the excited state reacts faster whereas this trend is reversed above 50 meV.

a new electronic channel becomes accessible, here the first vibrational state, $\text{N}_2^+(v=1)$, plays an important role as already discussed by several authors (see Ref. 8).

For the charge-transfer system $\text{Ar}^+ + \text{N}_2$, Fig. 7 shows a selection of results from several groups. Again we restrict the comparison to the $\sigma_{1/2}/\sigma_{3/2}$ ratio as a function of collision energy. Our data points (solid dots) are in satisfying agreement with the guided ion beam results from Ng's group (open squares) [21] and, at thermal energies, also with the drift tube results (crosses) [22], where they are usually rather reliable. Similar swarm experiments by Hamdan et al. [23] have resulted in similar values and are therefore omitted for clarity. Concerning the deviations in the energy dependence it should be noted that the drift field leads to a wide energy spread and that collisions with the buffer gas may also affect the internal states of the ions. In addition the swarm experiments have not been performed with state-selected ions but with a statistical mixture and state-specific information has been obtained by applying

the attenuation method. This procedure requires very accurate data, especially in instances like the present one, where the rate coefficients are almost equal. At collision energies above 1 eV there exist many other state-selected experiments [24–26]. These are likewise not reproduced in the figure since they all agree with the results of Ng and co-workers [21] within the error bars.

Further, for the $\text{Ar}^+ + \text{N}_2$ system the mass ratio and the experimental conditions are comparable to those of the $\text{Ar}^+ + \text{O}_2$ system and, in principle, trapping of primary ions due to inelastic scattering can lead to similar problems. However, the charge-transfer rate coefficient for thermalized ions is in this instance about a factor of ten smaller and therefore the measured cross-sections do not depend so critically on potential distortions of the octopole.

Our results clearly show that the spin-orbit state effects the reaction differently at low and high collision energies. Below 1 eV some state-specific calculations from Clary and Sonnenfroh [27] are known; however, they

have examined only the reaction with the $^2P_{3/2}$ state. Therefore we have only a speculative explanation for the measured low-energy behavior that the reaction is hindered by a barrier, and that fine-structure energy can help to surmount it. At energies above 1 eV theoretical investigations have been performed by Parlant and Gislason [28]. They have predicted the higher reactivity of the spin-orbit ground state as being due to an energy resonance between the $\text{Ar}^+ + \text{N}_2^+$ ($v=1$) channel and $\text{Ar}^+(^2P_{3/2}) + \text{N}_2$. Our experimental result, that the value of $\sigma_{1/2}/\sigma_{3/2}$ drops below 1 with increasing energy, is consistent with the threshold of 0.09 eV for formation of the $\text{N}_2^+(v=1)$ molecule.

To introduce the $\text{Ar}^+ + \text{N}_2$ charge-transfer reaction as a calibration standard would have the advantages that the cross-sections are bigger and that the quality of the data is much better as can be seen from the small error bars in Fig. 7. Besides that the absolute values are not so sensitive to the problem caused by trapped primary ions. Nonetheless we have chosen the $\text{Ar}^+ + \text{O}_2$ charge-transfer system because the relative effect of the spin-orbit states is much more pronounced, i.e. the cross-section ratio is 6:1 at $E_T = 0.4$ eV instead of only 2:3. In addition, the reaction with O_2 is far superior if one intends to determine small amounts of $^2P_{1/2}$ states in a ground-state Ar^+ beam.

3.5 $\text{Ar}^+ + \text{H}_2/\text{D}_2$

Among the systems we have studied, the strongest fine-structure dependence has been observed for the $\text{Ar}^+ + \text{H}_2$ charge transfer. Figure 8(a) shows the $\sigma_{1/2}/\sigma_{3/2}$ ratio for the H_2^+ channel while Fig. 8(b) depicts this ratio for the hydrogen abstraction reaction. At collision energies below 100 meV, the excited ion undergoes charge transfer with a cross-section which is 8 ± 1.5 times larger than that for the ground state. This pronounced fine-

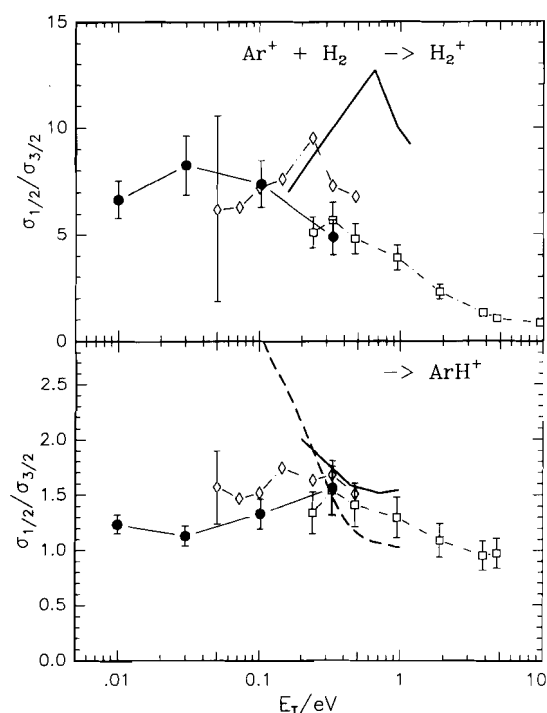


Fig. 8. Ratio of the cross-sections $\sigma_{1/2}$ and $\sigma_{3/2}$ as a function of the collision energy for the charge-transfer reaction $\text{Ar}^+ + \text{H}_2 \rightarrow \text{H}_2^+ + \text{Ar}$ (upper panel) and the reaction $\text{Ar}^+ + \text{H}^+ + 2 \rightarrow \text{ArH}^+ + \text{H}$ (lower panel) measured by several groups: Ng et al. [29] (\square); Tanaka et al. [32] (\diamond); this work (\bullet). The solid line shows the result from a theoretical investigation by Baer et al. [33]. The broken line represents the calculated ratio determined by Tosi et al. [34].

structure dependence has been explained by an energy resonance between the $\text{Ar}^+(^2P_{1/2})$ state and the $\text{H}_2^+(v^+ = 2)$ state [29]. Corresponding measurements which have been performed with deuterium as target gas are depicted in Fig. 9. For D_2 the energy levels are shifted such that there are no close resonances. Therefore the charge transfer is much less dependent on the ionic state and the ratio of the cross-sections remains below three. Furthermore, the cross-sections for forming ArH^+ and ArD^+ are only weakly dependent on the fine-structure state and, as can be seen in Figs. 8(b) and 9(b), the ratio $\sigma_{1/2}/\sigma_{3/2}$ lies only slightly above one.

Since from the systems we have studied, the

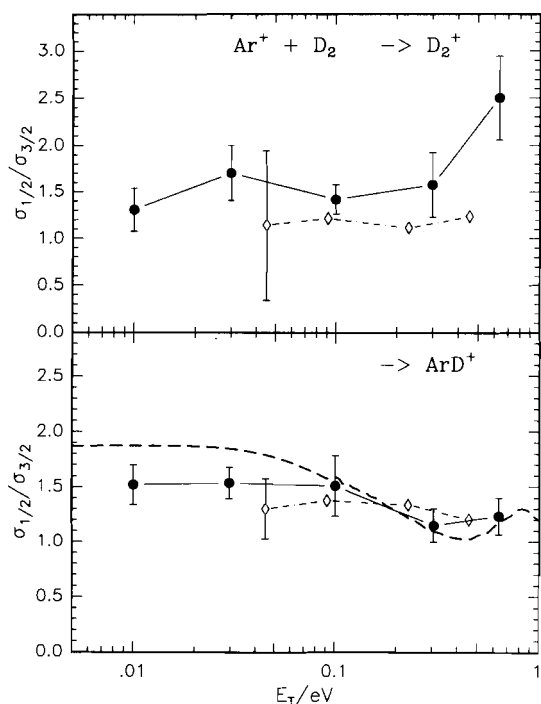


Fig. 9. Ratio of the cross-sections $\sigma_{1/2}$ and $\sigma_{3/2}$ as a function of the collision energy for the charge-transfer reaction $\text{Ar}^+ + \text{D}_2 \rightarrow \text{D}_2^+ + \text{Ar}$ (upper panel) and the reaction $\text{Ar}^+ + \text{D}_2^+ \rightarrow \text{ArD}^+ + \text{D}$ (lower panel) measured by several groups: Tanaka et al. [32] (O) this work (●). The broken line represents a theoretical prediction by Tosi et al. [34].

$\text{Ar}^+ + \text{H}_2$ charge-transfer system is the most sensitive process concerning the influence of spin-orbit energy it could be regarded as the best candidate for determining the $^2\text{P}_{1/2}/^2\text{P}_{3/2}$ ratio; however, this reaction is one of the most problematic ones from an experimental point of view. Firstly H_2^+ formation represents only a minor reaction channel since it competes with hydrogen abstraction and the ArH^+ products are formed roughly at the Langevin limit. An experimental problem is that the simultaneous confinement of H_2^+ products and Ar^+ primary ions requires operation of the guiding octopole at sufficiently high r.f. frequencies and amplitudes. Secondly, the H_2^+ ions produced have small kinetic energies, and thus potential distortions can easily lead to discrimination effects. More complica-

tions arise from the fact that both the ArH^+ and the H_2^+ products undergo secondary reactions with the H_2 target, and in both events the same product, H_3^+ , is formed. Our results have been corrected for this based on the known thermal rate coefficients of these reactions [30] and accounting for the mean flight time of the products through the scattering cell [31]. For the hydrogen abstraction channel corrections of only a few percent are necessary whereas the charge-transfer channel requires corrections between 10 and 30% depending on the spin-orbit state and the H_2/D_2 target.

Figures 8 and 9 show a selection of other experimental results and of theoretical predictions. In the overlapping energy range our experimental ratios are in good agreement with the results from Liao et al. [29]. There are some minor discrepancies between ours and those from Tanaka et al. [32]. For the ArH^+ channel the three-dimensional quantum mechanical calculation from Baer et al. [33] is in fairly good agreement with the experiments whereas significant deviations are obvious in the case of the charge transfer (Fig. 8(a)). A very recent experimental and theoretical investigation has been published by Tosi et al. [34]. These authors found, via a high-resolution beam experiment, an interesting structure in the energy dependence of the hydrogen abstraction cross-section which has been explained using a theoretical model. There are, however, some controversies since the structure could not be reproduced in an independent experiment [35,36]. Beyond that, the theoretical results from Ref. 34 give only a qualitative description of the reaction since the calculated absolute cross-sections are much smaller than the experimental results. Finally, also the theoretical $\sigma_{1/2}/\sigma_{3/2}$ ratios deviate significantly from the measurements as can be seen from the broken line in Fig. 8. Therefore, more experimental and theoretical work is needed for this very fundamental ion/molecule reaction.

The preceding comparisons and discussions have revealed that it is not straightforward to find an ideal reaction system for which the absolute values of state-specific cross-sections can be used for characterizing quantitatively the states populated in the various multi-photon ionization processes of Ar. Best agreements between results from different groups have been found for the charge transfer with nitrogen, but this system has the disadvantage that the cross-sections are only weakly dependent on the fine-structure state of the argon ion. More sensitive collision processes such as charge transfer with hydrogen or oxygen are rather problematic from an experimental point of view since they require an apparatus which is able to provide reliable information on integral cross-sections. This condition can be fulfilled, at least in principle, by the GIB method which can provide real 4π collection efficiency. However, this feature is not sufficient and the results of this work, among others, clearly demonstrate that the operation of a guided ion beam machine requires many tests and rigorous checks, the majority of which have been discussed in Ref. 7.

4. Conclusions

In this work, several REMPI schemes have been examined for preparing Ar^+ ions selectively in the two spin-orbit ground states. In contrast to the commonly used photoelectron spectroscopy, state-specific ion/molecule reactions have been used to determine the resulting $^2\text{P}_{3/2} : ^2\text{P}_{1/2}$ population. The proposed procedure to calibrate this ratio is based on the $\text{Ar}^+ + \text{O}_2$ charge-transfer process which shows a significant fine-structure dependence in the threshold region for forming the metastable $\text{O}_2^+(\text{a})$ ion. The use of a monitor reaction for characterizing reactants prepared in uncertain state distributions has the advantage that the ensemble is probed directly in the reaction

zone. It is evident that this method is limited to situations where only a few states are populated which is, however, often the case. We are currently using this method for probing ensembles which are thermalized at very low temperatures or photoionized with photon energies just above the ionization limit, and in situations where we intend to distinguish between electronic states, vibrational modes or different structures.

5. Acknowledgments

The authors thank Professors Smith and Schlier for many contributions and helpful discussions. Financial support of the Deutsche Forschungsgemeinschaft (Sonderforschungsbereich 276) is gratefully acknowledged.

6. References

- [1] W.A. Chupka and M.E. Russell, *J. Chem. Phys.*, 49 (1968) 5426.
- [2] K. Müller-Dethlefs and E.W. Schlag, *Annu. Rev. Phys. Chem.*, 42 (1991) 109.
- [3] F. Merkt, S.R. Mackenzie and T.P. Softley, *J. Chem. Phys.*, 99 (1993) 4213.
- [4] D. Smith and N.G. Adams, *Phys. Rev. A*, 23 (1981) 2327.
- [5] W. Lindinger, H. Villinger and F. Howorka, *Int. J. Mass Spectrom. Ion Phys.*, 41 (1981) 89.
- [6] J.D. Shao, Y.G. Li, G.D. Flesch and C.Y. Ng, *Chem. Phys. Lett.*, 132 (1986) 58.
- [7] D. Gerlich *Adv. Chem. Phys.*, 82 (1992) 1.
- [8] C.Y. Ng, *Adv. Chem. Phys.*, 82 (1992) 401.
- [9] S.L. Anderson *Adv. Chem. Phys.*, 82 (1992) 177.
- [10] C.E. Moore, National Standard Reference Data Series, National Bureau of Standards, Washington, 1971.
- [11] S.J. Bajic, *Ph.D. Thesis*, Oak Ridge National Laboratory Tennessee, TN, 1991.
- [12] T.M. Orlando, B. Yang and S.L. Anderson, *J. Chem. Phys.*, 90 (1989) 1577.
- [13] O. Dutuit, C. Alcaraz, D. Gerlich, P.M. Guyon, J. Hepburn, C. Métayer-Zeitoun, J.B. Ozenne, M. Schweizer and T. Weng, in preparation.
- [14] S. Scherbarth and D. Gerlich, *J. Chem. Phys.*, 90 (1989) 1610.

- [15] I. Dotan and W. Lindinger, *J. Chem. Phys.*, 76 (1982) 4972.
- [16] G.D. Flesch, S. Nourbakhsh and C.Y. Ng, *J. Chem. Phys.*, 92 (1990) 3590.
- [17] P.J. Chantry, *J. Chem. Phys.*, 55 (1971) 2746.
- [18] S.J. Bajic, R.N. Compton, X. Tang and P. Lambropoulos, *Phys. Rev. A*, 44 (1991) 2102.
- [19] T. Kato, *J. Chem. Phys.*, 80 (1984) 6105.
- [20] T. Matsuo, N. Kobayashi and Y. Kaneko, *J. Phys. Soc. Jpn.*, 55 (1986) 3045.
- [21] C.L. Liao, J.D. Shao, R. Xu, G.D. Flesch, Y.G. Li and C.Y. Ng, *J. Chem. Phys.*, 85 (1986) 3874.
- [22] T. Tobita, N. Kobayashi and Y. Kaneko, in J. Eichler, I.V. Hertel and N. Stolterfoth (Eds.), **XIII ICPEAC**, Int. Conference on the Physics of Electron and Atomic Collisions, 27 July–2 August 1983, Berlin.
- [23] M. Hamdan, K. Birkenshaw and N.D. Twiddy, *Int. J. Mass Spectrom. Ion Processes*, 57 (1984) 225.
- [24] T. Kato, K. Tanaka and I. Koyano, *J. Chem. Phys.*, 77 (1982) 337.
- [25] B.G. Lindsay and C.J. Latimer, *J. Phys. B*, 21 (1988) 1617.
- [26] P.M. Guyon, T.R. Govers and T. Baer, *Z. Phys. D*, 4 (1986) 89.
- [27] D.C. Clary and D.M. Sonnenfroh, *J. Chem. Phys.*, 90 (1989) 1686.
- [28] G. Parlant and E.A. Gislason, *J. Chem. Phys.*, 86 (1987) 6183.
- [29] C.L. Liao, R. Xu, S. Nourbakhsh, G.D. Flesch, M. Baer and C.Y. Ng, *J. Chem. Phys.*, 93 (1990) 4832.
- [30] Y. Ikezoe, S. Matsuoka, M. Takebe and A. Viggiano, *Gas Phase Ion–Molecule Reaction Rate Constants Through 1986*, published by Ion Reaction Research Group of the Mass Spectrometry Society of Japan, Tokyo, 1987, distributed by Maruzen Co.
- [31] M. Schweizer, **Ph.D. Thesis**, Universitat Freiburg, (1993).
- [32] K. Tanaka, J. Durup, T. Kato and I. Koyano, *J. Chem. Phys.*, 74 (1981) 5561.
- [33] M. Baer, C.L. Liao, R. Xu, S. Nourbakhsh, G.D. Flesch, C.Y. Ng and D. Neuhauser, *J. Chem. Phys.*, 93 (1990) 4845.
- [34] P. Tosi, O. Dmitrijev, Y. Soldo, D. Bassi, D. Cappelletti, F. Pirani and V. Aquilanti, *J. Chem. Phys.*, 99 (1993) 985.
- [35] D. Gerlich, H.J. Jitschin and O. Wick, in D. Bassi, M. Scotoni and P. Tosi (Eds.), *Symposium on Atomic and Surface Physics*, Pameago, 1992.
- [36] D. Gerlich, in T. Andersen, B. Fastrup, F. Folkmann and H. Knudsen and N. Andersen (eds.), *Electronic and Atomic Collisions*, invited paper on ICPEAC XVIII in Aarhus, 1993.
- [37] O. Dutuit, in K.R. Jennings, (ed.), *Proc. NATO Advanced Study Institutes on Fundamentals of Gas Phase Ion Chemistry 1990*, Kluwer, Dordrecht, 1991, p. 21.